Tropical Cyclone Intensity Estimation From Spaceborne Microwave Scatterometry and Parametric Wind Models

Weicheng Ni, *Student Member, IEEE*, Ad Stoffelen, *Fellow, IEEE*, Kaijun Ren, *Member, IEEE*, and Xiaofeng Yang, *Senior Member, IEEE*

***Abstract*—Spaceborne microwave sensors, measuring co-/cross-polarization (VV/VH) normalized radar cross section signals, have been widely used for tropical cyclone (TC) monitoring. However, considerable gaps remain to obtain TC intensity since these satellite data either blur inner-core structures (e.g., scatterometer data) or have limited spatial–temporal coverage (e.g., synthetic aperture radar (SAR) data). This study aims to get more accurate TC intensity estimates from scatterometers, which have good global coverage but relatively low spatial resolution. To overcome the blurring effect in scatterometers, we propose a new technique for guidance on TC intensities, with maximum 1-min sustained winds calculated as a function of decay parameters provided by the parametric Rankine-type model. The technique is employed on advanced scatterometer (ASCAT) data acquired between 2016 and 2017, validated with simultaneous SAR VH geophysical model function measurements and best-track (BT) estimates. When validated with BT estimates, the method enhances the blurred maximum winds, where the standard deviation of difference decreased from 6.3 to 3.49 m/s and the coefficient of determination increased from 0.7 to 0.89. Besides, it is noteworthy that the proposed technique performs slightly better than the Mayers–Ruf method. The promising results indicate that the technique can provide more representative TC maximum 1-min sustained wind estimates from ASCAT data, thus contributing to the further exploitation of scatterometer data for TC warnings.**

***Index Terms*—Blurring effect, maximum 1-min sustained wind, remote sensing, scatterometer, tropical cyclones (TCs).**

Manuscript received April 3, 2022; revised May 11, 2022; accepted May 27, 2022. Date of publication June 9, 2022; date of current version June 17, 2022. This work was supported in part by the National Key Research and Development Program of China under Grant 2018YFC1406206 and in part by the National Natural Science Foundation of China under Grant 61802424. The work of Ad Stoffelen was supported in part by the EUMETSAT OSI SAF. *(Corresponding author: Kaijun Ren.)*

Weicheng Ni is with the College of Meteorology and Oceanography, College of Computer Science and Technology, National University of Defense Technology, Changsha 410073, China, and also with the Department of Satellite Observations, Royal Netherlands Meteorological Institute, 3731GA De Bilt, The Netherlands (e-mail: niweicheng19@gmail.com).

Ad Stoffelen is with the Department of Satellite Observations, Royal Netherlands Meteorological Institute, 3731GA De Bilt, The Netherlands (e-mail: ad.stoffelen@knmi.nl).

Kaijun Ren is with the College of Meteorology and Oceanography, National University of Defense Technology, Changsha 410073, China (e-mail: renkaijun@nudt.edu.cn).

Xiaofeng Yang is with the State Key Laboratory of Remote Sensing Science, Aerospace Information Research Institute, Chinese Academy of Sciences, Beijing 100101, China (e-mail: yangxf@radi.ac.cn).

Digital Object Identifier 10.1109/JSTARS.2022.3180281

I. Introduction

TROPICAL cyclones (TCs) are rapidly rotating swirls over a small scale, along with a massive momentum exchange in the atmosphere and across the water–air interface. It is one of the most destructive natural disasters, bringing extreme wind force, heavy rain, large waves, and dramatic storm surges. The accurate knowledge of the TC strength and inner-core structure evolution will contribute to enhanced disaster responses by local governments.

In the past few decades, remote sensing technology has been widely used to provide large-scale real-time observations, especially in extreme conditions when *in situ* data are unavailable. The satellite-based Dvorak technique (DVKT) [1] is one of the most popular techniques for providing robust TC intensity information from satellite imagery, taking advantage of cloud patterns analysis [2]. However, the estimated results can easily deviate from real conditions because of the indirect measure and dispersion in cloud distributions [3], [4]. The evaluation by Knaff *et al.* [5] shows that the bias and root-mean-square error associated with DVKT wind estimates are a function of intensity, with a great limitation when estimating maximum wind speeds below 45 m/s and above 65 m/s. Moreover, users in other basins usually apply regional variations and modifications to the DVKT [6]. As a result, the method's general accuracy is subject to individual bias and human error.

Spaceborne microwave sensors, such as scatterometers, radiometers and synthetic aperture radars (SARs), have the unique capability of cloud penetration and can measure the ocean surface roughness information in all the weather conditions. SARs are capable of producing fine-scale spatial data [7], sensitive to extreme wind speeds up to 75 m/s with errors comparable to the collocated stepped frequency microwave radiometer (SFMR) measurements [8]. The fine space scale of SAR data makes it qualified to get an accurate averaged wind over 1 min, i.e., 1-min sustained wind. By contrast, the winds retrieved from scatterometers may be taken as about 10-min mean winds due to the relatively larger footprint. In some TC cases, the maximum 1-min sustained wind speed can be about 14% greater than the highest 10-min sustained wind over the same period [9]. Nevertheless, limited by the sporadic availability, hitherto SAR data cannot be used for global ocean TC monitoring or providing complete knowledge within a TC

This work is licensed under a Creative Commons Attribution 4.0 License. For more information, see https://creativecommons.org/licenses/by/4.0/

life cycle (TLC). The limitation of SAR makes it appealing to obtain accurate TC maximum 1-min sustained winds from scatterometer data, which measure co-polarized (VV/HH) normalized radar cross section (NRCS) signals at a relatively low resolution, but with good coverage. The advanced scatterometer (ASCAT) [10] provides 10-m stress-equivalent winds [11] on a swath grid of 12.5 km, providing good extreme wind speeds up to about 35 m/s [12]–[14]. To date, the ASCAT remains a critical surface wind source for TC forecast operations. It has proven to be very effective for wind vector retrieval [15] and has been extensively used in meteorological services [16]. It is worth noting that VV-retrieved wind speeds by the newly proposed CMOD7D geophysical model function (GMF) [17] can obtain values up to 70 m/s at good quality, exhibiting a remarkable capability of alleviating VV signal saturation issues though with uncertainty increasing when wind speeds are higher than 35 m/s. On the other hand, the blurring effect in the ASCAT remains due to the coarse resolution. In particular, when supervising TC phenomena, the inner structure will be largely blurred by its 20-km footprint, bringing in high wind speed errors near the eyewall. The estimation of actual TC intensity from coarse satellite data remains an open issue [18], [19]. For a more complete discussion of the limitations and future recommendations of scatterometer observations in TC cases, we refer to [20] and [21].

Past studies attempted to fit the existing parametric models to coarse observations in order to obtain more accurate TC metrics. For example, Chavas *et al.* [22] developed a complete radial wind structure model by merging the inner and outer wind structures. Morris and Ruf [23] fitted the parametric model to Cyclone Global Navigation Satellite System observations, which consist of collections of tracks rather than complete swaths. However, these studies focus on the limitations of the parametric models while paying less attention to the low resolution of the signal channels at high wind speeds. Reppucci *et al.* [24] set a wind speed threshold of 20 m/s when fitting the parametric Holland-type TC model to VV-derived wind speeds. Yet, the selection of a threshold of 20 m/s is arbitrary and rather low given recent studies [13], [14].

Observational studies indicate that the inner-core circulation appears to evolve nearly independently of the outer circulation, which coincides with the piecewise representation of Rankine-type wind function inside and beyond the eyewall [22], [25], [26]. As such, one can get two wind speed maxima from wind profiles inside and outside the eyewall separately. This study proposes a new approach to derive TC intensities, combining a parametric Rankine-type TC model and VV-retrieved high wind speeds (<35 m/s). The algorithm generates maximum 1-min sustained winds as a function of obtained two wind speed maxima and Rankine decay parameters so as to simulate the characteristic of the actual wind profile and solve the blurring effect. The ultimate goal of the study is to provide improved TC guidance based on many operational scatterometers (similar to ASCAT-A and ASCAT-B used in this study) in service of global TC monitoring. However, one primary obstacle to TC guidance from scatterometers is the indistinct TC structures. As such, some preliminary information regarding TC characteristics is required. To achieve this goal,

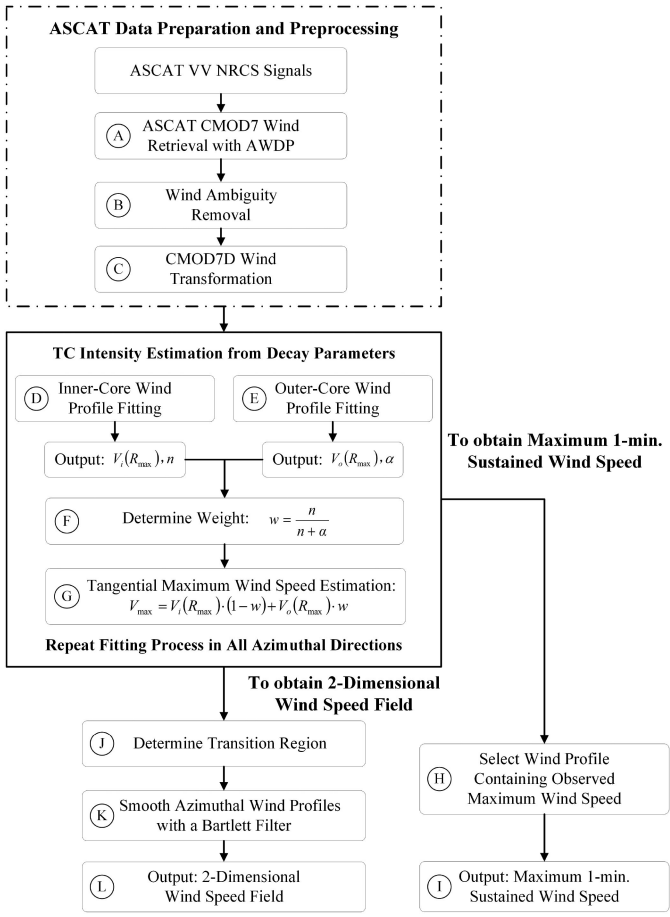

Fig. 1. Flowchart of TC intensity estimation using ASCAT VV signals.

the technique in this article is initially designed in the SAR TC images, which can provide prior knowledge of eyewall transition width and a preliminary evaluation of the method's feasibility and then extended to ASCAT data. Note that the suggested method can be independently used on ASCAT TC images when other wind references are absent. When extended to ASCAT data, the technique is validated by comparing ASCAT-retrieved results to TC intensity estimates from simultaneous SAR images and best-track (BT) data, revealing a satisfying improvement. In addition, it is worth mentioning that the calculated results are slightly better than the estimates from the Mayers–Ruf method [27]. The promising results contribute to our long-term goal of developing a general method for estimating TC maximum 1-min sustained winds for the plentiful scatterometer winds available for nowcasting. The flowchart of TC maximum 1-min sustained wind speed estimation from ASCAT VV signals is summarized in Fig. 1; this flowchart is identical to SAR VV signals.

The rest of this article is organized as follows. The datasets used in the study are described in Section II. Section III elaborates on the technique to estimate the TC maximum 1-min sustained wind speed and to construct the 2-D wind speed field with azimuthal dependence preserved. In Section IV, we present the estimation and validation results on ASCAT TC cases. Finally, Section V concludes this article.

II. Datasets

A. ASCAT Data

The ASCAT instruments are active microwave scatterometers aboard the MetOp satellites providing timely NRCS measurements with a nearly daily revisit time (subdaily after the launches of MetOp-B and MetOp-C) and nominal spatial sampling of 12.5 km [28], [29]. The ASCAT operates at C-band ($\sim$ 5.3 GHz) in VV polarization and uses six fan-beam antennas, three at each satellite side, to detect the ocean surface information. The individual antennas (fore, mid, and aft antenna) are orientated with respect to satellite track at azimuth angles of 45°, 90°, and 135°, respectively. All three antennas illuminate each point in the swath.

Sea surface roughness is an essential physical parameter in air–sea interaction studies, which connects the stress-equivalent 10-m-height wind speed U_{10S} with NRCS signals measured by satellite sensors. In the study, the ASCAT VV NRCS data were processed by the ASCAT wind data processor [30] for deriving ocean surface wind vectors from the radar measurements on a swath grid of 12.5 km. In the inversion step of wind retrieval, the CMOD7 GMF [12] is used to map a wind vector (specified in terms of wind speed and wind direction) to an NRCS value (box A in the flowchart of Fig. 1). CMOD7 is a state-of-the-art empirical model to relate the NRCS values to U_{10S}, used for operational wind scatterometry. Generally, there can be up to four ambiguous solutions, called ambiguities [31]. The ambiguous wind solutions in satellite images can be removed based on the cyclone characteristics: the winds blow counterclockwise around TC eyes in the Northern Hemisphere while clockwise in the Southern Hemisphere (box B).

CMOD7D [17] is adapted from CMOD7 with a polynomial transformation in the form of (1). CMOD7D results from a calibration toward SFMR winds of all collocated ASCAT winds up to 2019 [14], showing a strong correlation with the measured NRCS. Given these properties, CMOD7D is used to calibrate ASCAT CMOD7-derived winds following the wind speed reference de facto used in operational Hurricane advisories [13] (box C)

$$V_{7D} = 0.0095 * V_7^2 + 1.52 * V_7 - 7.6 \tag{1}$$

where V_{7D} and V_7 indicate the wind speeds provided to CMOD7D and CMOD7 GMFs, respectively. Particularly, when V_7 is smaller than 12 m/s, the obtained V_{7D} values should be ignored [14]. This phenomenon usually occurs in the relatively calm ocean areas. In this study, these V_{7D} values are replaced by the original V_7 wind speeds. Note that (1) essentially illustrates the uncertainty in the physical calibration of TC wind speeds due to inconsistency in the *in situ* wind speed references, while we here adhere to the dropsonde-based calibration standard used in operational TC forecasting for practical reasons to provide guidance on maximum 1-min sustained winds for operational TC advisories. Considering the high uncertainty of CMOD7D winds when wind speeds are higher than 35 m/s, the study estimates TC intensities using the most reliable high wind speeds retrieved from VV NRCS signals below 35 m/s.

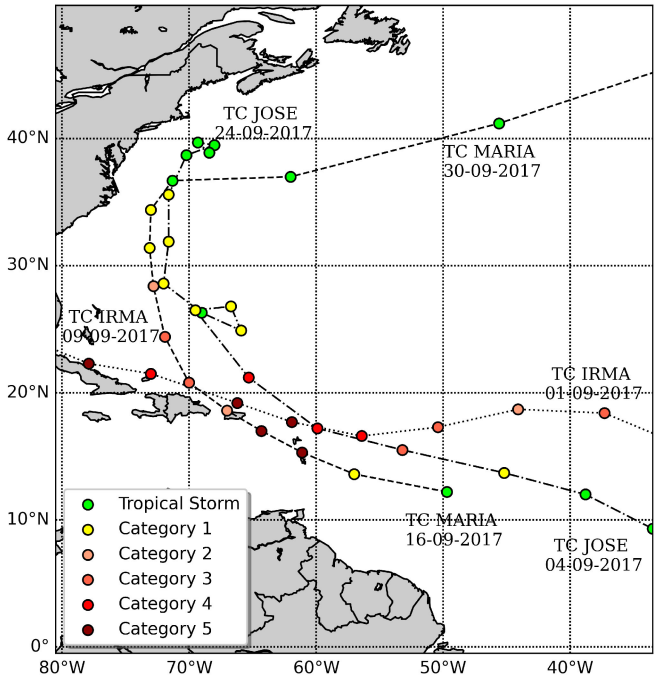

Fig. 2. Tracks of TCs (dashed line) Maria, (dotted line) Irma, and (dash-dotted line) Jose. The marker's color indicates TC category, provided by BT data and categorized according to the Saffir–Simpson Scale.

The study uses ASCAT TC observations from 2016 and 2017, for which the simultaneous Sentinel-1 (S1) SAR data with a time departure less than 3.5 h or BT data are accessible. Statistically, there were merely 19 TCs captured by S1 sensors between 2016 and 2017, with 35 images available in total. However, during the same period, the ASCAT sensors collected over 1000 images of the inner-core structures of TCs. The good global coverage of ASCAT data highlights the importance of obtaining more accurate TC metrics from ASCAT images.

B. S1 C-Band SAR Images

The Copernicus S1 mission provides complete C-band ($\sim$ 5.4 GHz) SAR operational applications and services. The two-satellite constellation of Sentinel-1A and 1B orbit Earth 180° apart, offering a global revisit time of around six days [32]. The first S1 SAR image of a TC was acquired in 2014, exhibiting an excellent ability for imaging fine-scale wind patterns on the sea surface beneath the clouds [7]. S1 SAR measurements uniquely capture TC inner-core characteristics to provide independent measurements of maximum wind speeds and radii of maximum wind speed (RMWs), verified by airborne SFMR winds. Taking the opportunity of the high resolution of SAR measurements, the method in this article is first constructed out of the SAR data, which can provide prior knowledge of the eyewall width; see Section III-D for details. The obtained knowledge can help users independently determine the eyewall width from ASCAT TC images.

As such, three S1 C-band SAR images on TCs Maria, Irma, and Jose are collected to describe the proposed new technique and retrieve the necessary information. SAR images are

TABLE I
S1 SAR IMAGERY INFORMATION OF TC CASES

TC Name	Acquisition Time	Image Mode	Centre Latitude	Centre Longitude	$\mathbf{V_{max}}$[a] Category[b]
Maria	21/09/2017 22:45	IW	20.7^oN	69.9^oW	63.2 m/s 4/5
Irma	07/09/2017 10:30	IW	20.0^oN	68.7^oW	76.9 m/s 5/5
Jose	08/09/2017 22:03	IW	16.6^oN	58.5^oW	66.3 m/s 4/5

[a]Maximum wind speeds at the acquisition time, estimated by MS1AHW GMF from SAR images.
[b]TC categories at the acquisition time and their highest category levels during the TLCs.

acquired in interferometric wide (IW) swath mode, allowing images with 250-km-wide swath and incidence angles ranging from 30° to 46°. Fig. 2 shows the tracks of three TCs, with locations determined by BT data [33] and categories by the Saffir–Simpson scale. TC information at the acquisition time is presented in Table I. SAR TC winds are retrieved with MS1AHW GMF [8], [34].

Apart from the three S1 SAR images described above, other 16 SAR images (when simultaneous ASCAT measurement are also available) are used for evaluating the maximum 1-min sustained winds retrieved from collocated ASCAT data (see Section IV). For TC information, refer to Table II.

C. BT Data

The International Best Track Archive for Climate Stewardship (IBTrACS) dataset is one of the most comprehensive global databases of past TC data. The dataset was developed by the NOAA National Climatic Data Center, which combines existing BT data spanning from the 1840s to present from over ten international forecast centers [33]. The study uses the latest version 4 of IBTrACS [35] for cyclone tracks visualization (see Section II-B) and TC intensity references preparation (see Section IV). When employing the proposed technique to the ASCAT dataset, the TC center locations and intensities in the IBTrACS dataset are interpolated to image acquisition times.

III. METHODOLOGY

A. Idealized Tangential Wind Profile Formulation

TC tangential wind profiles are often smoothed or approximated by continuous analytic functions with adjustable parameters, which are physically meaningful [36], [37]. Historical parametric wind functions used in TC cases include the parametric Holland model [38], [39] and the Rankine-type model [40]. The Holland model approximates TC profiles as a family of rectangular hyperbolas in terms of surface pressures. However, this analytical representation suffers from systematic errors: the magnitude of the second derivative of the wind with respect to radius is too small near the RMW where the profile is concave downward and too large away from the maximum where the profile is concave upward [41].

The parametric Rankine-type function, not suffering from the limitations above, is selected in the study. The wind speeds are proportional to a power of radius inside the eyewall and decay gradually away from the storm center with respect to the decay parameters, which control the shape of wind profiles [36]. Assuming that there is only one wind speed maximum (the single-modified Rankine vortex, SMRV), the transition across the eyewall (i.e., the eyewall width) is smoothed with a polynomial ramp function [42] so that the profile has continuous radial derivatives [43]

$$V(r) = V_i(r) = V_{\max}\left(\frac{r}{R_{\max}}\right)^n, \qquad (0 \le r \le R_1) \quad (2a)$$

$$V(r) = V_i(r)\,[1 - w(r)] + V_o(r)w(r), \quad (R_1 \le r \le R_2) \quad (2b)$$

$$V(r) = V_o(r) = V_{\max}\left(\frac{R_{\max}}{r}\right)^\alpha, \qquad (R_2 \le r) \quad (2c)$$

where V_i and V_o are tangential wind speeds inside and beyond the transition region; $V_{\max}$ and $R_{\max}$ are the maximum 1-min sustained wind speed and radius, respectively, where the inflection points occur; and r is the radius. Parameters n and α are decay parameters for inner and outer wind profiles, respectively. The transition region lies between $r = R_1$ and $r = R_2$, where $R_1 \le R_{\max} \le R_2$.

w is a bellramp transition function, which ramps up smoothly from zero to one between R_1 and R_2, defined as

$$w_4(\xi) = 126\,\xi^5 - 420\,\xi^6 + 540\,\xi^7 - 315\,\xi^8 + 70\,\xi^9 \quad (3)$$

where ξ is a nondimensional argument expressed in the form of $\xi = (r - R_1)/(R_2 - R_1)$. When $\xi \le 0, w = 0$; when $\xi \ge 1, w = 1$.

The traditional parametric SMRV model is one of the most commonly used functions, which can approximate wind profile well when accurate maximum wind speed and transition region width are provided. However, the actual maximum wind speeds are often underestimated due to the signal saturation phenomenon and blurring effect by coarse spatial resolution. Besides, the knowledge of R_1 and R_2 locations is currently missing; thus, the accuracy is subject to human error. The study selects CMOD7D GMF for alleviating the VV signal saturation issue. In order to deal with the blurring effect, we propose a new method for actual maximum sustained wind speed retrieval, taking advantage of the Rankine decay parameters (see Sections III-B and III-C). The high spatial resolution of the SAR measurements can provide a prior for transition width (see Section III-D).

B. Wind Profile Fitting

TC center identification is the first step prior to the wind profile fitting. The centers in SAR images are estimated using the gray-level gradient co-occurrence matrix method, which detects the calm TC eye area by texture analysis [44]. The parametric model SMRV approximates the TC as a vortex with single primary circulation with four parameters $V_{\max}$, $R_{\max}$, α and n, expressed by (2). $R_{\max}$ is determined by scanning each profile for

TABLE II
MAXIMUM WIND SPEEDS CALCULATED FROM ASCAT DATA AND THOSE FROM SIMULTANEOUS SAR DATA

NO.	Acquisition Time	Name	Cyclone Location	Centre Lat	Centre Lon	Category	SAR Type	SAR MS1AHW	ASCAT Type	ASCAT CMOD7D	This Study
1	2016-08-26	Lester	EPA	17.6^oN	115.2^oW	2	S1A	42.2 m/s	ASCAT-B	33.3 m/s	39.5 m/s
2	2016-08-26	Lester	EPA	17.6^oN	115.3^oW	2	S1A	42.2 m/s	ASCAT-A	36.9 m/s	36.9 m/s
3	2016-08-31	Lester	EPA	17.7^oN	137.0^oW	4	S1A	64.0 m/s	ASCAT-B	50.9 m/s	55.8 m/s
4	2016-08-31	Lester	EPA	17.7^oN	137.1^oW	4	S1A	64.0 m/s	ASCAT-A	54.4 m/s	56.2 m/s
5	2016-08-27	Lionrock	WPA	26.1^oN	136.6^oE	4	S1A	60.0 m/s	ASCAT-A	51.4 m/s	57.9 m/s
6	2016-08-28	Lionrock	WPA	26.4^oN	136.8^oE	4	S1A	60.0 m/s	ASCAT-B	50.5 m/s	56.8 m/s
7	2016-08-29	Lionrock	WPA	32.3^oN	143.3^oE	1	S1A	37.4 m/s	ASCAT-A	42.2 m/s	48.3 m/s
8	2016-08-29	Lionrock	WPA	32.5^oN	143.3^oE	1	S1A	37.4 m/s	ASCAT-B	42.1 m/s	40.7 m/s
9	2016-08-30	Lionrock	WPA	36.1^oN	142.5^oE	4	S1A	58.3 m/s	ASCAT-A	53.9 m/s	58.2 m/s
10	2016-08-30	Gaston	ATL	31.4^oN	54.9^oW	2	S1A	45.9 m/s	ASCAT-A	36.9 m/s	37.9 m/s
11	2016-08-30	Gaston	ATL	31.5^oN	54.8^oW	2	S1A	45.9 m/s	ASCAT-B	40.4 m/s	43.3 m/s
12	2016-09-02	Gaston	ATL	38.9^oN	33.1^oW	4	S1A	62.5 m/s	ASCAT-A	39.7 m/s	50.8 m/s
13	2016-09-02	Gaston	ATL	38.9^oN	32.8^oW	4	S1A	62.5 m/s	ASCAT-B	42.1 m/s	52.8 m/s
14	2016-09-05	Hermine	ATL	37.3^oN	68.3^oW	1	S1A	42.2 m/s	ASCAT-B	35.8 m/s	36.9 m/s
15	2016-09-05	Hermine	ATL	38.8^oN	68.7^oW	1	S1A	37.9 m/s	ASCAT-A	30.7 m/s	33.7 m/s
16	2016-09-05	Hermine	ATL	38.9^oN	68.8^oW	1	S1A	37.9 m/s	ASCAT-B	33.4 m/s	34.8 m/s
17	2016-09-24	Karl	ATL	30.5^oN	65.3^oW	2	S1A	49.3 m/s	ASCAT-B	35.7 m/s	38.3 m/s
18	2016-09-24	Karl	ATL	30.7^oN	65.2^oW	2	S1A	49.3 m/s	ASCAT-A	36.5 m/s	39.9 m/s
19	2017-02-07	Carlos	IND	19.3^oS	55.5^oE	1	S1A	35.4 m/s	ASCAT-B	30.4 m/s	35.0 m/s
20	2017-02-13	Dineo	IND	21.3^oS	39.9^oE	TS	S1A	23.5 m/s	ASCAT-B	28.4 m/s	30.8 m/s
21	2017-02-13	Dineo	IND	21.3^oS	39.9^oE	TS	S1A	23.5 m/s	ASCAT-A	34.0 m/s	30.8 m/s
22	2017-09-05	Katia	EPA	22.3^oN	97.1^oW	TS	S1A	17.2 m/s	ASCAT-B	14.3 m/s	16.8 m/s
23	2017-09-05	Katia	EPA	22.4^oN	97.1^oW	TS	S1A	17.2 m/s	ASCAT-A	27.3 m/s	30.0 m/s
24	2017-09-18	Maria	ATL	14.6^oN	59.9^oW	3	S1A	54.8 m/s	ASCAT-A	46.3 m/s	48.8 m/s
25	2017-09-22	Maria	ATL	20.9^oN	70.1^oW	4	S1A	67.7 m/s	ASCAT-A	54.2 m/s	59.1 m/s
26	2017-10-14	Ophelia	ATL	36.0^oN	23.5^oW	3	S1B	50.0 m/s	ASCAT-B	55.9 m/s	52.8 m/s

Cyclone locations are eastern Pacific (EPA), western Pacific (WPA), Atlantic (ATL), and Indian Ocean (IND). SAR types are Sentinel-1A (S1A) and Sentinel-1B (S1B). ASCAT types are ASCAT-A and ASCAT-B.

the strongest wind and its radial position. This procedure leaves the SMRV model with three parameters that can be obtained by least-squares fitting to the data.

As a piecewise parametric model, one can get two $V_{\max}$ values from inner (V_i) and outer (V_o) wind profiles by minimizing the cost functions (box D and box E in Fig. 1)

$$S^2 = \sum_{k=1}^{K} \left[v_0\left(r_k\right) - v_g\left(r_k, \alpha, R_{\max}\right)\right]^2, \quad \begin{matrix} R_{\max} \le r_k, \\ v_0 \le 35 \text{ m/s} \end{matrix} \tag{4a}$$

$$S^2 = \sum_{k=1}^{K} \left[v_0(r_k) - v_g\left(r_k, n, R_{\max}\right)\right]^2, \quad \begin{matrix} r_k \le R_{\max} \\ v_0 \le 35 \text{ m/s} \end{matrix} \tag{4b}$$

where $v_0(r_k)$ and $v_g(r_k)$ indicate the observed and simulated wind speed values at the radial distance of r_k, respectively.

Since the parameter space has relatively few dimensions and the cost function is essentially a parabola, we use the simplex algorithm [45] to find the minimum value of S^2. The black curves in Fig. 3(a) represent two wind profiles fitted from the inner and outer VV-retrieved CMOD7D wind vector cells (WVCs) in TC Maria. WVCs are resolution elements of the measured swath, wherein the winds are estimated independently [46]. The purple and green shadow areas stand for the reliable portions of inner and outside wind profiles (with wind speeds below the threshold of 35 m/s) utilized for wind profile fitting and the maximum 1-min sustained wind speed estimation. Notably, the observed wind speed profiles generally deviate from SMRV at some distance from the vortex, as shown in the gray area (named the outer-vortex region) in Fig. 3. It is commonly due to the effect of eyewall replacement cycles (ERCs), spiraling convection bands or landfalling. In study, it is necessary to exclude these outer-vortex regions when fitting the wind profiles. This study takes advantage of the shape-preserving characteristics of the Savitzky–Golay smoothing filter [47] to obtain the overall shapes of the wind profiles while ignoring the smallest scales. The filter achieves the smoothing of signals by using a simplified least-squares-fit convolution. After that, the outer-vortex region can be easily identified according to the reduction in the wind gradients.

C. Maximum 1-min Sustained Wind Speed Estimation From Rankine Decay Parameters

Reppucci *et al.* [24] estimated the TC intensities using SAR VV images, combined with a parametric Holland-type model. However, the selection of a threshold of 20 m/s is slightly arbitrary, and only the area outside the eyewall is used. In practice, it can bring overfitting and overestimation issues during the maximum 1-min sustained wind speed estimation procedure. To solve this problem, the study first separately generates wind profiles inside and beyond eyewall out of reliable WVCs. This process returns $V_i(R_{\max})$ and $V_0(R_{\max})$, i.e., the maximum wind speeds for inner and outer wind profiles at eyewall locations. The final maximum 1-min sustained wind speed can be obtained requiring that $V_i(R_{\max}) = V_0(R_{\max})$. This

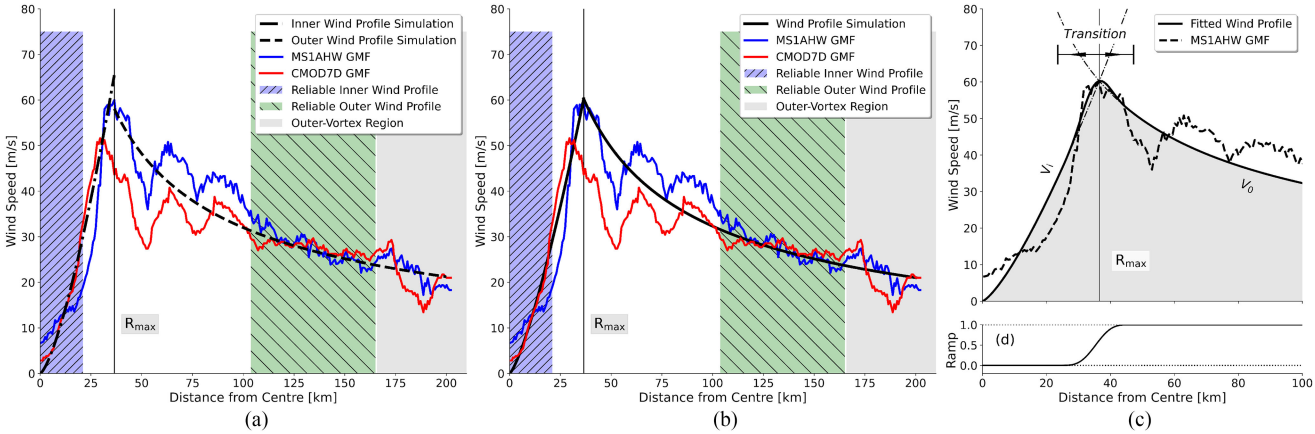

Fig. 3. (a) SAR-retrieved wind speed profiles and wind speed profile simulations (black curves) for a transect of TC Maria. The colors of the curves indicate wind speed profiles calculated with different GMFs. The purple and green shadow regions show the reliable wind regions, which are used for profile fitting. The gray region indicates the outer-vortex region, which needs to be cut out. (b) Actual maximum 1-min sustained wind speed calculated from Rankine decay parameters. (c) Transition region across the eyewall. The dashed curve indicates the wind profile calculated with the MS1AHW GMF, which is considered the real reference. (d) Polynomial ramp weighting function used to smooth the transition region between the inner and outer profiles.

condition yields the value of weight w at $r = R_{\max}$ as (box F)

$$w\left(\frac{R_{\max}-R_1}{R_2-R_1}\right)=\frac{\frac{\partial V_i}{\partial r}}{\frac{\partial V_i}{\partial r}-\frac{\partial V_0}{\partial r}}=\frac{n}{n+\alpha}. \tag{5}$$

Following that, the true maximum 1-min sustained wind speed is computed as (box G)

$$V_{\max}=V_i\left(R_{\max}\right)\frac{\alpha}{n+\alpha}+V_0\left(R_{\max}\right)\frac{n}{n+\alpha}. \tag{6}$$

With $V_{\max}$ value determined, one can refit parametric model to CMOD7D winds, in combination of (2a), (2c), and (4). The solid black curve in Fig. 3(b) presents the simulated wind profile. As can be observed, the maximum wind speed retrieved from SAR VV signals with the proposed technique is closer to SAR VH GMF measurements, i.e., the MS1AHW GMF curves in Fig. 3.

In the study, the wind profiles containing CMOD7D-retrieved maximum 10-min mean winds are selected for the fitting procedure (box H) and TC maximum 1-min sustained wind speed estimation (box I). However, the classical SMRV model is designed to be radially symmetric, failing to preserve the azimuthal variations in the TC structure. In addition, accurate transition widths are usually unknown. These drawbacks make it difficult to construct reasonable 2-D wind speed images. Therefore, a newly designed method is described in the following sections (see Sections III-D and III-E), which preserves the eyewall structure and the TC asymmetric features when simulating the wind speeds.

D. Transition Area

Wind profiles falling within the transition region can be generated as follows: First, determine the location of the transition region. Generally, the width of transition $R_1 - R_2$ can be specified as *a priori* at a value between 10 and 25 km [42]. Wind profiles with different transition widths are drawn in Fig. 4. A sharper peak will occur with transition region width decreasing. The optimal transition region width is supposed to relate to the values of RMW. Root-mean-square differences (RMSDs)

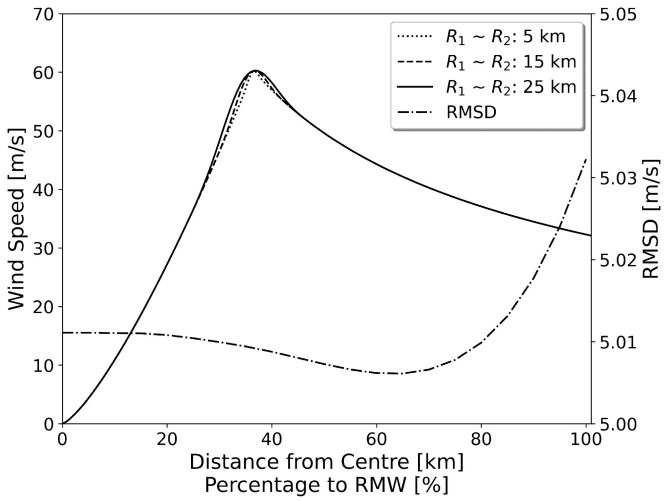

Fig. 4. Wind speed profiles with different transition region widths. The right axis represents RMSDs between fitted results and MS1AHW measurements, with transition region widths determined as percentages of RMW values.

between fitted wind speeds and MS1AHW measurements are calculated (the dash-dotted line in Fig. 4), with transition region widths determined as different percentages of RMW values. As can be observed, the RMSD goes down first and reaches the minimum at around 65%; then, it increases dramatically. Note that the local minimum can be unclear in some TC cases where RMSD values increase monotonically. Further study is necessary to explore the relationship between the transition widths and RMW values. In the study, the transition region widths are defined as 65% of RMW values.

Combining the weight w at $r = R_{\max}$ (5) and the polynomial expression of the weighting function $w_4(\xi)$ (3), one can determine R_1 and R_2 locations (box J) and then the wind profile over the transition region with (2 b), as shown in Fig. 3(c). The wind profile calculated with MS1AHW GMF [the dashed curve in Fig. 3(c)] is also plotted, which is in high agreement with

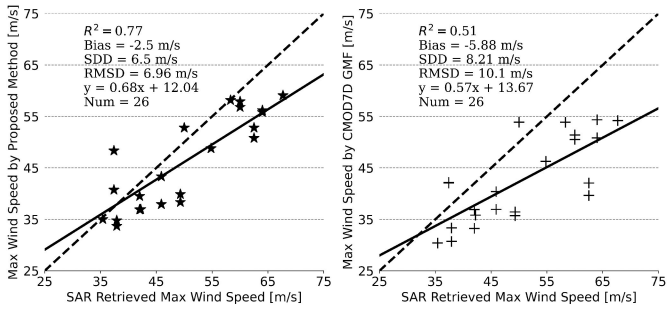

Fig. 5. (a) Scatter plot of ASCAT-retrieved (with the proposed technique) maximum 1-min sustained wind speeds versus the SAR-retrieved maximum 1-min sustained wind speeds. (b) Scatter plot of ASCAT-retrieved (CMOD7D-based) maximum 10-min mean wind speeds versus the SAR-retrieved maximum 1-min sustained wind speeds.

the fitted wind profile. Fig. 3(d) shows the weighting function values, $w_4(\xi)$, over the transition region.

E. Smooth Over Neighboring Wind Profiles

In order to preserve the TC's azimuthal dependence, the technique repeats the profile fitting process for observed wind speed profiles at different azimuthal directions, with an interval of 10°. The interval of 10° is the compromise between computation cost and the accuracy of TC structure. After that, the estimated azimuthal maximum wind speeds and relevant parameters n, α, R_1, and R_2 (2) are smoothed with a 60° (six points) Bartlett filter for the desired effect of reducing transient peaks [40] (box K).

IV. Results and Discussions

It is noteworthy that the method has been satisfactorily tested on SAR VV signals for TCs Maria, Irma, and Jose. The VV-retrieved results with the proposed method are more in line with the SAR VH GMF measurements than the original VV CMOD7D estimates (not shown in this article). The technique can reduce the mean bias from -12.61 to -8.32 m/s and the standard deviation of difference (SDD) from 9.14 to 7.3 m/s. These experimental results prove the credibility of the method.

This section exploits the proposed method in ASCAT TC images to obtain maximum 1-min sustained wind speed estimates, validated by simultaneous SAR measurements and BT data. Ten TC cases with 26 available SAR-ASCAT image pairs are used, with a time departure less than 3.5 h. TC cases selected are listed in Table II, in which both the satellite sensors captured TC centers.

As reported in Table II, the maximum 1-min sustained wind speed estimates from ASCAT data (with the proposed technique) are closer to the values measured by SAR images than ASCAT CMOD7D-based results. A scatter plot of the estimated maximum 1-min sustained wind speeds versus the SAR-retrieved maximum 1-min sustained wind speeds is shown in Fig. 5(a). The coefficient of determination (R^2) is 0.77, while the bias is -2.5 m/s, the SDD is 6.5 m/s, and the RMSD is 6.96 m/s. Fig. 5(b) shows the scatter plot of ASCAT CMOD7D-based maximum 10-min mean wind speeds versus the SAR-retrieved speeds, with R^2 of 0.51, the bias of -5.88 m/s, the SDD of 8.21 m/s, and the RMSD of 10.1 m/s. The RMSD of 6.96 m/s in Fig. 5(a) may look unimpressive compared to the maximum 1-min sustained wind speeds derived from other satellite sensors (e.g., see [48, Table V]), which perhaps attributed to the uncertainty of SAR data at extreme winds [49]. In addition, the retrieval and GMF errors in SAR winds, which we deemed the reference wind in the study, are ignored.

The right panels in Fig. 6 present TC wind speed images retrieved with the proposed technique from ASCAT data. For comparison, ASCAT TC wind images simulated by the parametric SMRV model (the left panels in Fig. 6) and those estimated by the CMOD7D GMF [see Fig. 6(b), (f), and (j)] are added. The panels on the third column in Fig. 6 [see Fig. 6(c), (g), and (k)] display collocated SAR wind speed images using MS1AHW GMF. All these wind speed maps can display TC inner structures well. Yet, in contrast with the CMOD7D-based [see Fig. 6(b), (f), and (g)] and SMRV-simulated [see Fig. 6(a), (e), and (i)] ASCAT TC images, the proposed technique can further enhance TC inner structures, generating TC wind images closer to those in simultaneous SAR data.

After that, the validation of the proposed technique is extended to more ASCAT TC images acquired in the TC seasons (from May 1st to October 31st) of 2016 and 2017. The obtained maximum 1-min sustained wind speeds from ASCAT data are compared with the counterparts provided by the BT dataset. In the study, only the TC cases with maximum wind speeds higher than 30 m/s, i.e., TC categories (by the Saffir–Simpson scale) greater than or equal to 1, are selected. There are 346 cases available in total. Fig. 7(a) shows the scatter plot of the estimated maximum 1-min sustained wind speeds (hereafter noted as V_E) versus BT-provided estimates (hereafter noted as V_{BT}), while Fig. 7(b) shows the scatter plot of the ASCAT CMOD7D-based maximum 10-min mean wind speeds (hereafter noted as V_{C7D}) versus V_{BT}.

On purpose to make a better case for the proposed method, the true maximum wind speeds by the Mayers–Ruf method [27] are calculated (hereafter noted as V_M), as shown in Fig. 7(c). Mayers and Ruf constructed a correction algorithm to scale the coarsely resolved wind speed measurements (V_R) to true maximum sustained wind speeds

$$V_M = SF_R(R_{\max}, V_R) \cdot V_R \tag{7}$$

where $SF_R(R_{\max}, V_R)$ indicates scale factors sensitive to changes in storm sizes (RMWs, noted as $R_{\max}$) and TC intensities (V_R) observed by satellites.

The method, appearing to be more general and less limited than other methods, can be used to further evaluate our approach. The red solid curves in Fig. 7(a)–(c) stand for the maximum wind speed estimates from three different approaches. Fig. 7(d) shows the biases of wind speeds by three methods with respect to BT estimates. Fig. 7(b) reveals an apparent saturation phenomenon for V_{C7D} values, especially when V_{BT} values are higher than 35 m/s. Subsequently, the V_{C7D} estimates continue saturating and finally level off at around 55 m/s, smaller than the corresponding V_{BT} values, as expected. The rapid growing bias values in Fig. 7(d) (the black curve) prove the saturation phenomenon

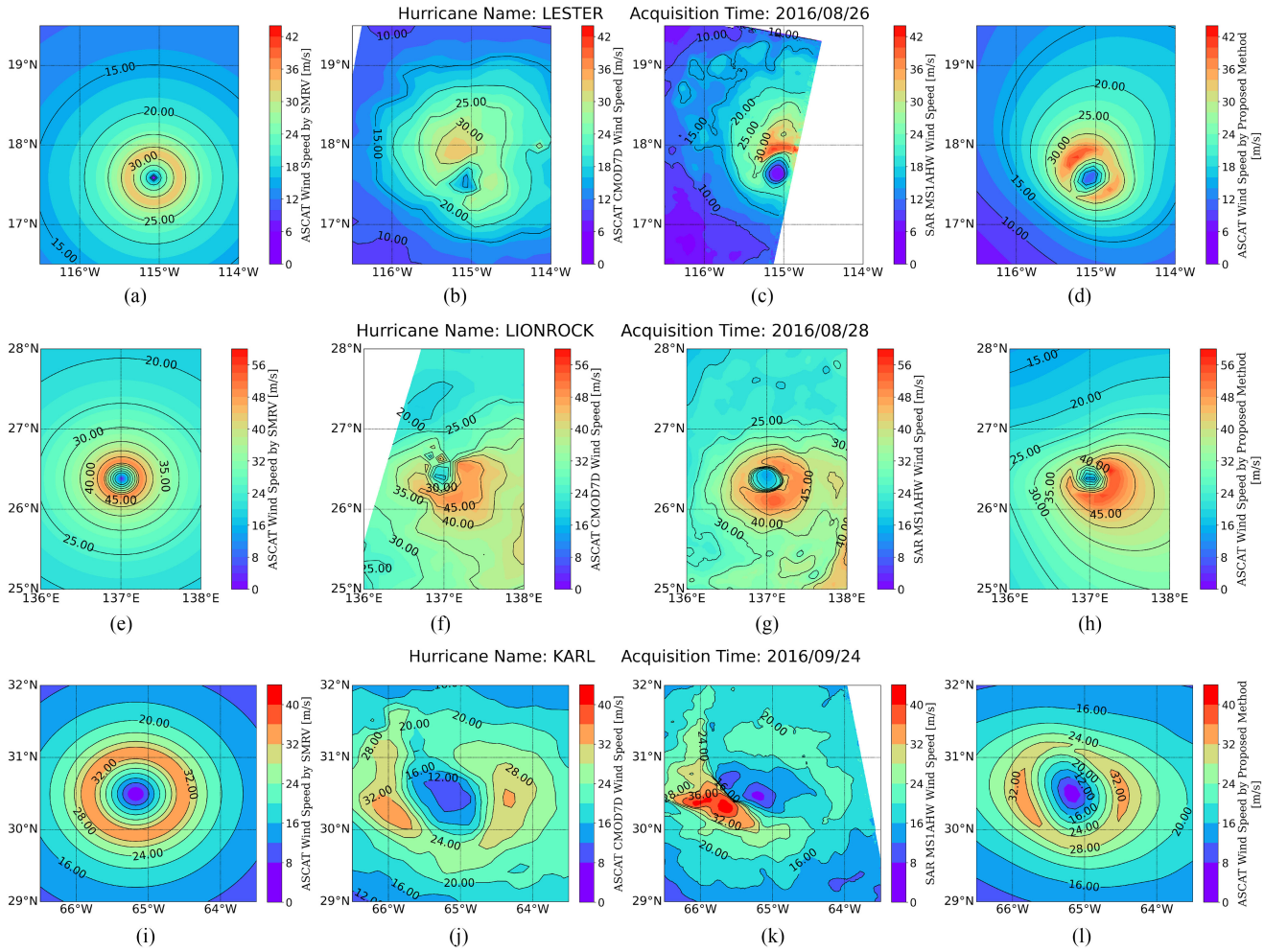

Fig. 6. Left panels: ASCAT TC wind speed images simulated by the parametric model SMRV [(a), (e), and (i)]. Middle panels: TC wind speed images retrieved from ASCAT data with CMOD7D GMF [(b), (f), and (j)] and collocated SAR wind speed images [(c), (g), and (k)] by MS1AHW GMF with a time departure less than 3.5 h. Right panels: TC wind speed images retrieved from ASCAT data using the proposed technique [(d), (h), and (l)].

in CMOD7D results. In [13] and [14], the effect of spatial resolution on underestimating maximum 1-min sustained winds by moderate resolution sensors such as ASCAT is addressed. It confirms that the CMOD7D GMF is consistent with the BT speed reference, while ASCAT is of insufficient spatial resolution to depict maximum 1-min sustained eyewall winds. On the other hand, the estimates by the proposed technique, as well as the Mayers–Ruf method, increase linearly with V_{BT}, being slightly larger than V_{BT} values. In Fig. 7(a), R^2 is 0.89, the SDD is 3.49 m/s, and the RMSD is 4.27 m/s, superior to the original CMOD7D results (with R^2 of 0.7, the SDD of 6.3 m/s, and the RMSD of 7.2 m/s). Besides, it is worth mentioning that the proposed method performs slightly better than the Mayers–Ruf method, in which R^2 is 0.85, the SDD is 4.76 m/s, and the RMSD is 5.01 m/s. Note that the estimates by the Mayers–Ruf method can be inaccurate in the extreme wind speed regime (>60 m/s). Compared to the estimates by the technique in this article, the maximum wind speeds by the Mayers–Ruf method have higher bias values (behave as the underestimation), as the blue curve in Fig. 7(d) presents. The unique characteristic reflects that the proposed technique can further alleviate the low sensitivity issue at extreme winds and, meanwhile, return more representative maximum 1-min sustained wind speeds.

The overall results show that the proposed technique is able to obtain a more precise estimate of the TC intensity from ASCAT data. It will contribute to TC explorations using scatterometer data, which have global coverage, but relatively low spatial resolution. The proposed method makes an improvement to the traditional parametric Rankine-type model, with the maximum wind speed estimated as a function of Rankine decay parameters, so as to obtain more representative maximum 1-min sustained wind speeds from ASCAT data. On purpose to preserve the TC azimuthal dependence, the wind profile fitting process is repeated in all the azimuthal directions and a Bartlett filter is used to make a smooth over the neighboring radial wind profiles. The overall results above show that the proposed technique is able to enhance the blurred TC intensities in ASCAT VV NRCS signals. However, the method remains to be improved. One main limitation of the parametric Rankine model is that the model-calculated wind speed may match well with observations at the location selected, yet not for another location [50]. Similar to the single-exponential profile noted in [42], small values of

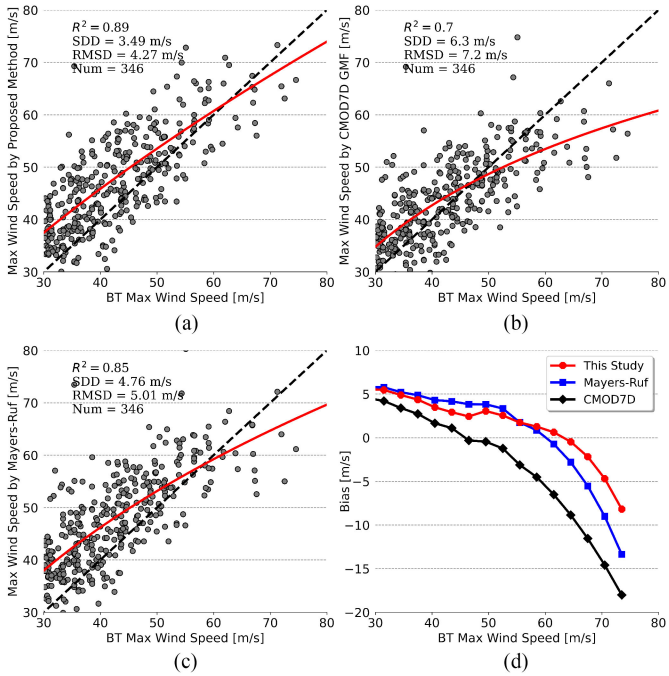

Fig. 7. (a) and (b) Scatter plot of ASCAT-retrieved (with the proposed technique/CMOD7D-based) maximum 1-min sustained wind speeds versus BT products. (c) Scatter plot of maximum 1-min sustained wind speeds by the Mayers–Ruf method versus BT products. Red solid curves in (a)–(c) stand for the maximum wind speed estimates from different methods. (d) Biases of three methods with respect to BT estimates.

exponent α may fail to capture the rapid decrease of wind just outside the eyewall; conversely, large exponent α values generate profiles that match the steep gradient outside the eyewall but decrease too rapidly farther away from the center. In practice, the signal integration over a relatively large area for ASCAT data results in highly smooth over observed wind profiles, making it possible to find an acceptable value for exponent α. The usage of the Rankine-type function for maximum 1-min sustained wind speed calculation, therefore, appears reasonable. However, it deserves to see if some more complex models, such as the dual-exponential wind profile [42] and ER11 [51], can perform better. On the other hand, the classical parametric SMRV model is constructed in the form of radially symmetric. Though the study designed a new method for preserving the azimuthal dependence, it is still worth exploring whether some asymmetric parametric TC models [52], [53] can have better performance. Moreover, some challenges remain, especially when TCs go through an ERC or have double eyewalls. The current model cannot deal with these complex TCs, and such conditions should be subject to further research.

V. Conclusion

Scatterometers have a good capability of global TC tracking but are of insufficient spatial resolution to depict the maximum 1-min sustained winds due to the large footprint. The study seeks to better exploit the plentiful ASCAT TC acquisitions by developing guidance to estimate the maximum 1-min sustained wind speeds as used in advisories. To achieve this goal, we propose a new method for obtaining more representative maximum 1-min sustained wind speeds, with estimates calculated as a function of Rankine decay parameters.

The technique is employed on ASCAT TC images, validated by simultaneous SAR MS1AHW measurements and BT-provided TC intensities. The satisfying agreement between ASCAT-derived maximum 1-min sustained wind speeds and SAR/BT estimates proves the technique's feasibility, which can alleviate VV signal saturation issues at extreme winds and the blurring effect by scatterometer footprints. The reliability of the proposed method in ASCAT data is also supported by comparing our technique to the Mayers–Ruf method.

To sum up, this study presents a brief contribution to TC intensity estimation with first results that look very encouraging. The successful experimental results suggest that the general application of the method for scatterometer winds is a promising long-term goal for obtaining 1-min sustained winds. Therefore, in future studies, the work will extend to all TCs archived by the Satellite Hurricane Observation Campaign and associated tests for the plentiful operational scatterometer data to devise a scheme for operational implementation. At that time, different scatterometer systems (e.g., RapidScat and OSCAT) and scatterometer products in various resolutions (e.g., ASCAT ultrahigh-resolution wind products on a 5.6-km grid size) will be tested.

Acknowledgment

Most datasets used in this study are provided by the EUMETSAT OSI SAF. The authors would like to acknowledge the European Space Agency and the French Research Institute for Exploitation of the Sea for Sentinel-1 data obtained through the Satellite Hurricane Observation Campaign and support through the MAXSS project. The authors would like to thank Gerd-Jan van Zadelhoff for help in accessing the Sentinel-1 data and Jur Vogelzang for providing valuable suggestions for this article.

References

[1] T. L. Olander and C. S. Velden, "The advanced Dvorak technique: Continued development of an objective scheme to estimate tropical cyclone intensity using geostationary infrared satellite imagery," *Weather Forecast.*, vol. 22, no. 2, pp. 287–298, 2007.

[2] C. Velden *et al.*, "The Dvorak tropical cyclone intensity estimation technique: A satellite-based method that has endured for over 30 years," *Bull. Amer. Meteorol. Soc.*, vol. 87, no. 9, pp. 1195–1210, 2006.

[3] X. Li *et al.*, "Tropical cyclone morphology from spaceborne synthetic aperture radar," *Bull. Amer. Meteorol. Soc.*, vol. 94, no. 2, pp. 215–230, 2013.

[4] Y. Pan, A. K. Liu, S. He, J. Yang, and M.-X. He, "Comparison of typhoon locations over ocean surface observed by various satellite sensors," *Remote Sens.*, vol. 5, no. 7, pp. 3172–3189, 2013.

[5] J. A. Knaff, D. P. Brown, J. Courtney, G. M. Gallina, and J. L. Beven, "An evaluation of Dvorak technique-based tropical cyclone intensity estimates," *Weather Forecast.*, vol. 25, no. 5, pp. 1362–1379, 2010.

[6] C. Velden *et al.*, "Supplement: The Dvorak tropical cyclone intensity estimation technique a satellite-based method that has endured for over 30 years," *Bull. Amer. Meteorol. Soc.*, vol. 87, no. 9, pp. S6–S9, 2006.

[7] X. Li, "The first Sentinel-1 SAR image of a typhoon," *Acta Oceanologica Sinica*, vol. 34, no. 1, pp. 1–2, 2015.

[8] A. Mouche, B. Chapron, J. Knaff, Y. Zhao, B. Zhang, and C. Combot, "Copolarized and cross-polarized SAR measurements for high-resolution description of major hurricane wind structures: Application to irma category 5 hurricane," *J. Geophys. Res.: Oceans*, vol. 124, no. 6, pp. 3905–3922, 2019.

[9] J.-H. Chu, *Intensity Observation and Forecast Errors*. Philadelphia, PA, USA: United States Navy, 1999, sec. 2.

[10] J. Figa-Saldaña, J. J. Wilson, E. Attema, R. Gelsthorpe, M. R. Drinkwater, and A. Stoffelen, "The advanced scatterometer (ASCAT) on the meteorological operational (METOP) platform: A follow on for European wind scatterometers," *Can. J. Remote Sens.*, vol. 28, no. 3, pp. 404–412, 2002.

[11] J. de Kloe, A. Stoffelen, and A. Verhoef, "Improved use of scatterometer measurements by using stress-equivalent reference winds," *IEEE J. Sel. Topics Appl. Earth Observ. Remote Sens.*, vol. 10, no. 5, pp. 2340–2347, May 2017.

[12] A. Stoffelen, J. A. Verspeek, J. Vogelzang, and A. Verhoef, "The CMOD7 geophysical model function for ASCAT and ERS wind retrievals," *IEEE J. Sel. Topics Appl. Earth Observ. Remote Sens.*, vol. 10, no. 5, pp. 2123–2134, May 2017.

[13] A. Stoffelen *et al.*, "C-band high and extreme-force speeds (CHEFS)—Final report," 2020. [Online]. Available: www.eumetsat.int/CHEFS

[14] F. Polverari *et al.*, "On high and extreme wind calibration using ASCAT," *IEEE Trans. Geosci. Remote Sens.*, vol. 60, 2022, Art. no. 4202210.

[15] J. Vogelzang, A. Stoffelen, A. Verhoef, and J. Figa-Saldaña, "On the quality of high-resolution scatterometer winds," *J. Geophys. Res.: Oceans*, vol. 116, no. C10, 2011 Art. no. C10033.

[16] A. Stoffelen, R. Kumar, J. Zou, V. Karaev, P. S. Chang, and E. Rodriguez, "Ocean surface vector wind observations," in *Remote Sensing of the Asian Seas*. New York, NY, USA: Springer, 2019, pp. 429–447.

[17] A. Stoffelen *et al.*, "Hurricane ocean wind speeds," in *Proc. EGU Gen. Assem. Conf. Abstr.*, 2021, Art. no. EGU21-11075.

[18] N. Reul *et al.*, "A revised L-band radio-brightness sensitivity to extreme winds under tropical cyclones: The five year SMOS-storm database," *Remote Sens. Environ.*, vol. 180, pp. 274–291, 2016.

[19] T. Meissner, L. Ricciardulli, and F. J. Wentz, "Capability of the SMAP mission to measure ocean surface winds in storms," *Bull. Amer. Meteorol. Soc.*, vol. 98, no. 8, pp. 1660–1677, 2017.

[20] M. J. Brennan, C. C. Hennon, and R. D. Knabb, "The operational use of QuikSCAT ocean surface vector winds at the national hurricane center," *Weather Forecast.*, vol. 24, no. 3, pp. 621–645, 2009.

[21] J. A. Knaff *et al.*, "Estimating tropical cyclone surface winds: Current status, emerging technologies, historical evolution, and a look to the future," *Trop. Cyclone Res. Rev.*, vol. 10, no. 3, pp. 125–150, 2021.

[22] D. R. Chavas, N. Lin, and K. Emanuel, "A model for the complete radial structure of the tropical cyclone wind field. Part I: Comparison with observed structure," *J. Atmos. Sci.*, vol. 72, no. 9, pp. 3647–3662, 2015.

[23] M. Morris and C. S. Ruf, "Determining tropical cyclone surface wind speed structure and intensity with the CYGNSS satellite constellation," *J. Appl. Meteorol. Climatol.*, vol. 56, no. 7, pp. 1847–1865, 2017.

[24] A. Reppucci, S. Lehner, J. Schulz-Stellenfleth, and S. Brusch, "Tropical cyclone intensity estimated from wide-swath SAR images," *IEEE Trans. Geosci. Remote Sens.*, vol. 48, no. 4, pp. 1639–1649, Apr. 2010.

[25] A. C. Didlake, Jr., and R. A. Houze, Jr., "Convective-scale variations in the inner-core rainbands of a tropical cyclone," *J. Atmos. Sci.*, vol. 70, no. 2, pp. 504–523, 2013.

[26] A. C. Didlake and R. Houze, "Dynamics of the Stratiform sector of a tropical cyclone rainband," *J. Atmos. Sci.*, vol. 70, no. 7, pp. 1891–1911, 2013.

[27] D. Mayers and C. Ruf, "Estimating the true maximum sustained wind speed of a tropical cyclone from spatially averaged observations," *J. Appl. Meteorol. Climatol.*, vol. 59, no. 2, pp. 251–262, 2020.

[28] L. Brocca *et al.*, "A review of the applications of ASCAT soil moisture products," *IEEE J. Sel. Topics Appl. Earth Observ. Remote Sens.*, vol. 10, no. 5, pp. 2285–2306, May 2017.

[29] M. El Hajj *et al.*, "Evaluation of SMOS, SMAP, ASCAT and Sentinel-1 soil moisture products at sites in southwestern France," *Remote Sens.*, vol. 10, no. 4, 2018, Art. no. 569.

[30] *ASCAT Wind Product User Manual, version 1.16, EUMETSAT OSI KNMI SAF, De Bilt*, The Netherlands, 2019. [Online]. Available: https://scatterometer.knmi.nl/

[31] J. Vogelzang and A. Stoffelen, "ASCAT ultrahigh-resolution wind products on optimized grids," *IEEE J. Sel. Topics Appl. Earth Observ. Remote Sens.*, vol. 10, no. 5, pp. 2332–2339, May 2017.

[32] *Introducing Sentinel-1, Eur. Space Agency,* Paris, France. [Online]. Available: https://www.esa.int/Applications/Observing_the_Earth/Copernicus/Sentinel-1/Introducing_Sentinel-1/. Accessed: May 12, 2022.

[33] K. R. Knapp, M. C. Kruk, D. H. Levinson, H. J. Diamond, and C. J. Neumann, "The International Best track archive for climate stewardship (IBTrACS): Unifying tropical cyclone data," *Bull. Amer. Meteorol. Soc.*, vol. 91, no. 3, pp. 363–376, 2010.

[34] A. A. Mouche, B. Chapron, B. Zhang, and R. Husson, "Combined co-and cross-polarized SAR measurements under extreme wind conditions," *IEEE Trans. Geosci. Remote Sens.*, vol. 55, no. 12, pp. 6746–6755, Dec. 2017.

[35] K. R. Knapp, J. P. K. Diamond, J. Howard, M. C. Kruk, and C. J. Schreck, *International Best Track Archive for Climate Stewardship (IBTrACS) Project, Version 4*. Asheville, NC, USA: NOAA National Centers for Environmental Information, 2018.

[36] M. Sitkowski, J. P. Kossin, and C. M. Rozoff, "Intensity and structure changes during hurricane eyewall replacement cycles," *Monthly Weather Rev.*, vol. 139, no. 12, pp. 3829–3847, 2011.

[37] G. Zhang, B. Zhang, W. Perrie, Q. Xu, and Y. He, "A hurricane tangential wind profile estimation method for C-band cross-polarization SAR," *IEEE Trans. Geosci. Remote Sens.*, vol. 52, no. 11, pp. 7186–7194, Nov. 2014.

[38] G. J. Holland, "An analytic model of the wind and pressure profiles in hurricanes," *Monthly Weather Rev.*, vol. 108, no. 8, pp. 1212–1218, 1980.

[39] G. Holland, "A revised hurricane pressure–wind model," *Monthly Weather Rev.*, vol. 136, no. 9, pp. 3432–3445, 2008.

[40] K. J. Mallen, M. T. Montgomery, and B. Wang, "Reexamining the near-core radial structure of the tropical cyclone primary circulation: Implications for vortex resiliency," *J. Atmos. Sci.*, vol. 62, no. 2, pp. 408–425, 2005.

[41] H. Willoughby and M. Rahn, "Parametric representation of the primary hurricane vortex. Part I: Observations and evaluation of the Holland (1980) model," *Monthly Weather Rev.*, vol. 132, no. 12, pp. 3033–3048, 2004.

[42] H. Willoughby, R. Darling, and M. Rahn, "Parametric representation of the primary hurricane vortex. Part II: A new family of sectionally continuous profiles," *Monthly Weather Rev.*, vol. 134, no. 4, pp. 1102–1120, 2006.

[43] S. Zieger, J. D. Kepert, D. J. Greenslade, and S. Aijaz, "Assessment of tropical cyclone wave models for engineering applications," *Ocean Eng.*, vol. 225, 2021, Art. no. 108748.

[44] W. Ni, A. Stoffelen, and K. Ren, "Hurricane eye morphology extraction from SAR images by texture analysis," *Front. Earth Sci.*, vol. 16, pp. 190–205, 2022.

[45] J. A. Nelder and R. Mead, "A simplex method for function minimization," *Comput. J.*, vol. 7, no. 4, pp. 308–313, 1965.

[46] H. Schultz, "A circular median filter approach for resolving directional ambiguities in wind fields retrieved from spaceborne scatterometer data," *J. Geophys. Res.: Oceans*, vol. 95, no. C4, pp. 5291–5303, 1990.

[47] A. Savitzky and M. J. Golay, "Smoothing and differentiation of data by simplified least squares procedures," *Anal. Chem.*, vol. 36, no. 8, pp. 1627–1639, 1964.

[48] K. Xiang, X. Yang, M. Zhang, Z. Li, and F. Kong, "Objective estimation of tropical cyclone intensity from active and passive microwave remote sensing observations in the northwestern pacific ocean," *Remote Sens.*, vol. 11, no. 6, 2019, Art. no. 627.

[49] M. Gade and A. Stoffelen, "An introduction to microwave remote sensing of the Asian Seas," in *Remote Sensing of the Asian Seas*. New York, NY, USA: Springer, 2019, pp. 81–101.

[50] L. Vijayan, W. Huang, K. Yin, E. Ozguven, S. Burns, and M. Ghorbanzadeh, "Evaluation of parametric wind models for more accurate modeling of storm surge: A case study of Hurricane Michael," *Natural Hazards*, vol. 106, no. 3, pp. 2003–2024, 2021.

[51] K. Emanuel and R. Rotunno, "Self-stratification of tropical cyclone outflow. Part I: Implications for storm structure," *J. Atmos. Sci.*, vol. 68, no. 10, pp. 2236–2249, 2011.

[52] M. Olfateh, D. P. Callaghan, P. Nielsen, and T. E. Baldock, "Tropical cyclone wind field asymmetry—Development and evaluation of a new parametric model," *J. Geophys. Res.: Oceans*, vol. 122, no. 1, pp. 458–469, 2017.

[53] S. Wang *et al.*, "An improved asymmetric hurricane parametric model based on cross-polarization SAR observations," *IEEE J. Sel. Topics Appl. Earth Observ. Remote Sens.*, vol. 14, pp. 1411–1422, 2021.

Weicheng Ni (Student Member, IEEE) received the B.S. degree in geophysical information science from Zhejiang University, Hangzhou, China, in 2017. He is currently working toward the Ph.D. degree with the National University of Defense Technology, Changsha, China.

He is a Visiting Scholar with the Royal Netherlands Meteorological Institute, De Bilt, The Netherlands, and is working on the intercalibration between scatterometer data and synthetic aperture radar data.

Ad Stoffelen (Fellow, IEEE) received the M.Sc. degree in physics from the Technical University of Eindhoven, Eindhoven, The Netherlands, in 1987, and the Ph.D. degree in meteorology on scatterometry from the University of Utrecht, Utrecht, The Netherlands, in 1998.

He currently leads a group on active satellite sensing with the Royal Netherlands Meteorological Institute, De Bilt, The Netherlands, and is involved in topics from future missions and retrieval to 24/7 operations, user training, and services. He is also deeply involved in the European Space Agency ADM-Aeolus Doppler Wind Lidar mission.

Kaijun Ren (Member, IEEE) received the B.S. degree in applied mathematics in 1998 and the M.S. and Ph.D. degrees in computer science in 2003 and 2008, respectively, all from the National University of Defense Technology, Changsha, China.

He is currently a Professor with the College of Meteorology and Oceanography and the College of Computer, National University of Defense Technology. His current research interests include high-performance computing, cloud computing, big data, and their interdisciplinary applications in ocean science and meteorology areas.

Xiaofeng Yang (Senior Member, IEEE) received the B.S. degree in environmental science from Sichuan University, Chengdu, China, in 2005, and the Ph.D. degree in cartography and geographic information systems from the Institute of Remote Sensing Applications (IRSA), Chinese Academy of Sciences (CAS), Beijing, China, in 2010.

From 2009 to 2010, he was a Visiting Research Scientist with the Department of Atmospheric and Oceanic Science, University of Maryland, College Park, MD, USA. In 2010, he joined IRSA, CAS, where he became an Associate Professor in 2013 and a Full Professor in 2016. His research interests include satellite oceanography, synthetic aperture radar image processing, and marine atmospheric boundary layer process studies.

Dr. Yang is an Associate Editor for *Remote Sensing* and an Editorial Board Member of IEEE TRANSACTIONS ON GEOSCIENCE AND REMOTE SENSING. He is the Secretary General of the Technical Committee on Earth Science from Space, Chinese Society of Space Research.